Taylor & Francis
Taylor & Francis Group

Check for updates

Near wall motion of undulatory swimmers in non-Newtonian fluids

Gaojin Li and Arezoo M. Ardekani

School of Mechanical Engineering, Purdue University, West Lafayette, IN, USA

ABSTRACT

We investigate the near-wall motion of an undulatory swimmer in both Newtonian and non-Newtonian fluids using a two-dimensional direct numerical simulation. Our results show that the undulatory swimmer has three types of swimming mode depending on its undulation amplitude. The swimmer can be strongly attracted to the wall and swim in close proximity of the wall, be weakly attracted to the wall with a relatively large distance away from the wall, or escape from the wall. The scattering angle of the swimmer and its hydrodynamic interaction with the wall are important in describing the near-wall swimming motion. The shear-thinning viscosity is found to increase the swimming speed and to slightly enhance the wall attraction by reducing the swimmer's scattering angle. The fluid elasticity, however, leads to strong attraction of swimmer's head towards the wall, reducing the swimming speed. The combined shear-thinning effect and fluid elasticity results in an enhanced swimming speed along the wall.

1. Introduction

Near-surface accumulation of micro-organisms have been widely observed for spermatozoa (Rothschild, 1963; Woolley, 2003), bacteria (Lauga, DiLuzio, Whitesides, & Stone, 2006), *C. elegans* (Yuan, Raizen, & Bau, 2015) and algae (e.g. *Chlamydomonas*) (Kantsler, Dunkel, Polin, & Goldstein, 2013). Many different effects are involved in the wall-induced attraction of swimming micro-organisms. The far-field hydrodynamic effects on a swimmer depend on the swimmer type. A pusher, which generates thrust behind its body such as most bacteria, is attracted to the wall when swimming parallel to the surface. A puller, on the other hand, reorients itself in the direction perpendicular to the surface (Berke, Turner, Berg, & Lauga, 2008; Spagnolie & Lauga, 2012). Other studies have showed that the orientational Brownian diffusion and intrinsic swimming stochasticity enhance the wall accumulation (Drescher, Dunkel, Cisneros, Ganguly, & Goldstein, 2011; Li & Tang, 2009). More details on the near wall motion of swimmers in the

---

Stokes regime can be found in recent review articles (Elgeti, Winkler, & Gompper, 2015; Lauga & Powers, 2009). Beyond the Stokes regime, small but non-negligible inertial effects has been considered by Li and Ardekani (2014).

When a swimmer gets close to a wall, the short-range hydrodynamic interaction and the contact with the wall are important in accurate prediction of the near-surface behaviour. Experiments show that the contact between the cilia and the surface determines the scattering behaviour of bull spermatozoa and *Chlamydomonas* algae from a solid boundary (Kantsler et al., 2013). Spermatozoa accumulate close to a surface (Rothschild, 1963). Their flagella beat in a three-dimensional waveform of conical shape or in a nearly planar wave form (Woolley, 2003). Numerical simulations show that the near-wall swimming motion of a sperm depends on its initial location and angle (Smith, Gaffney, Blake, & Kirkman-Brown, 2009). The wall attraction of the sperm is affected by the flagellar wavenumber but not the shape of the head (Ishimoto & Gaffney, 2014). It swims at a distance of about the swimmer size away from the wall (Smith et al., 2009). Wall attraction of a sperm is also observed in the simulations based on the multi-particle collision dynamics (Elgeti, Kaupp, & Gompper, 2010). However, these results show that the sperm is in a close contact with the wall. A sperm, whose flagellum has chiral asymmetry, swims in a circular trajectory (Elgeti et al., 2010). A circular trajectory was also observed for bacteria swimming near a wall (Lauga et al., 2006). For a hyper-activated sperm, its large undulation amplitude and asymmetric waveform greatly affect the near-wall motion and the binding dynamics to the wall (Curtis, Kirkman-Brown, Connolly, & Gaffney, 2012; Simons, Olson, Cortez, & Fauci, 2014).

The fluid environment of micro-organisms is often complex and shows both shear-thinning and viscoelastic properties (Hwang, Litt, & Forsman, 1969; Wolf, Blasco, Khan, & Litt, 1977). Such examples can be found in bacteria within biofilms which occur on different surfaces (Hall-Stoodley, Costerton, & Stoodley, 2004), the spermatozoa in the female reproductive tract swimming through the cervical mucus (Suarez & Pacey, 2006), *H. pylori* colonising the mucus layer covering the stomach (Montecucco & Rappuoli, 2001) and *B. burgdorferi* penetrating the connective tissues in the skin (Harman et al., 2012). The effects of fluid elasticity on the micro-organisms swimming speed in an unbounded domain have been widely investigated. Depending on the swimming strategy, flexibility of the flagellum, and the rheological properties of the background fluid, both speed enhancement and reduction have been observed (Lauga, 2007; Shen & Arratia, 2011; Teran, Fauci, & Shelley, 2010; Thomases & Guy, 2014; Li & Ardekani, 2015). For a finite planer flagellum, the speed enhancement due to the fluid elasticity occurs for a soft kicker with an amplitude increasing from its head to the tail (Thomases & Guy, 2014). However, it should be noted that the speed of a soft undulatory flagellum is much smaller than a stiff swimmer (Guy & Thomases, 2015).

Recent studies show that shear-thinning viscosity have an important effect on the micro-organism swimming behaviour (Li & Ardekani, 2015; Vélez-Cordero, & Lauga, 2013). A peak in the swimming speed of bacteria at a certain polymer concentration was observed in a solution of high molecular weight polymers (Martinez et al., 2014). The enhanced swimming speed of bacteria is found to be related to the reduced viscosity encountered by its fast-rotating flagella instead of fluid elasticity (Martinez et al., 2014). For a *C. elegans* in a shear-thinning fluid, its swimming speed and kinematics are less affected by the shear-thinning behaviour of the fluid, while its flow field and power consumption are greatly modified (Gagnon, Keim, & Arratia, 2014; Gagnon & Arratia, 2016). A similar behaviour is observed using the analysis of small amplitude waving sheet (Vélez-Cordero, & Lauga, 2013). Numerical simulations, on the other hand, show speed enhancement of a sperm in a shear-thinning fluid (Montenegro-Johnson, Smith, & Loghin, 2013; Montenegro-Johnson, Smith, Smith, Loghin, & Blake, 2012). Our recent studies illustrate that the speed enhancement occurs at large oscillation amplitudes as an undulatory flagellum creates a corridor of low-viscosity fluid around it, leading to a similar effect as confinement (Li & Ardekani, 2015). The relationship proposed by Li and Ardekani for the swimmer's energy consumption in a shear-thinning fluid is recently experimentally observed for *C. elegans* (Gagnon & Arratia, 2016). A spherical squirmer, on the other hand, may swim faster and slower in a shear-thinning fluid depending on the slip velocity on its surface (Datt, Zhu, Elfring, & Pak, 2015).

Proximity to a wall greatly affects the motion of a micro-organism in both Newtonian and non-Newtonian fluids. Analytical results show that an infinitely long flagellum swims faster but less efficient when close to a wall in a Newtonian fluid (Katz, 1974). This speed enhancement is weakened by the fluid elasticity (Chrispell, Fauci, & Shelley, 2013). These studies of infinitely long flagellum does not consider wall attraction, which can be important for bacteria and spermatozoa. The wall effects on the motion of passive particles in viscoelastic and shear-thinning fluids have been extensively studied (Ardekani, Joseph, Dunn-Rankin, & Rangel, 2009; Ardekani, Rangel, & Joseph, 2007; Li, McKinley, & Ardekani, 2015). However, the near-wall swimming of a self-propelled micro-organism in non-Newtonian fluids is still poorly understood. The analytical results for a squirmer showed that the fluid elasticity leads to an emergence of a limit cycle for pushers and pullers near a wall and changes the center fixed points to unstable foci. (Yazdi, Ardekani, & Borhan, 2015). For a squirmer with an oscillating tangential surface velocity, both pullers and pushers in a viscoelastic fluid swim towards the no-slip boundary if they are initially located within a small attraction region near the wall (Yazdi, Ardekani, & Borhan, 2014). In a fluid with strong fluid elasticity, direct numerical simulations showed that the neutral squirmer in viscoelastic fluids stays near a wall for a longer time compared to a Newtonian fluid, while a puller is less affected. A pusher is found to be trapped near the

wall because of a highly stretched region of polymer molecules formed behind its body (Li, Karimi, & Ardekani, 2014).

In this work, we investigate the near-wall motion of an undulatory swimmer in Newtonian and non-Newtonian fluids using a two-dimensional direct numerical simulation. We simulate the swimmer as a finite-length flagellum with a kinematically specified waving form, and two types of swimmer, kicker and burrower, are studied to model the sperm and *C. elegans*, respectively. Wall attraction of the swimmer as well as its effect on the swimming performance is analysed. The effects of shear-thinning fluid viscosity and fluid elasticity on the near-wall swimming dynamics are considered. In particular, we find that an enhanced swimming speed can be achieved by a combination of wall effects, fluid elasticity and shear-thinning viscosity.

2. Mathematical model and numerical method

2.1. Governing equations

We model the swimmer as a two-dimensional flagellum of finite length immersed in a fluid. An undulatory swimmer with its waving plane perpendicular to the wall were observed for sperm (Kantsler et al., 2013) and *C. elegans* (Yuan et al., 2015). The prescribed motion of the waving flagellum (Taylor, 1951) is given by a travelling wave $y = a(s)\cos[2\pi(s/l - t/T)]$, where t is the time, $a(s)$ is the dimensionless amplitude, l is the swimmer length and $s \in [0, l]$ is the length measured from the head of the swimmer. In all our results, the length is scaled by l, time by the waving time period T, velocity by l/T, and pressure and stress by μ/T, where μ is the fluid dynamic viscosity. Two undulatory swimming types are considered by varying the undulation amplitude along the swimmer. For the kicker, its amplitude linearly increases from the head to tail as $a(s) = As/l$, and for the burrower, the undulation amplitude decreases towards the tail as $a(s) = A(1 - s/l)$. At length and velocity scales relevant to micro-organisms, inertial effects are neglected. The dimensionless equations for conservation of momentum and mass are

$$Re\frac{D\boldsymbol{u}}{Dt} = -\nabla p + \nabla \cdot \boldsymbol{\tau} + \boldsymbol{f}, \qquad \nabla \cdot \boldsymbol{u} = 0, \tag{1}$$

where $\boldsymbol{u}$ is the velocity vector, p is the pressure and $\boldsymbol{\tau}$ is the deviatoric stress tensor. For micro-organisms, the Reynolds number $Re = \rho l^2/T\mu$ is negligible, where ρ is the fluid density. In this study, the Reynolds number is set to $Re = 6.25 \times 10^{-3}$. The forcing term $\boldsymbol{f}$, calculated using a distributed Lagrange multiplier method (Ardekani, Dabiri, & Rangel, 2008; Li & Ardekani, 2015), is used to ensure the no-slip boundary condition on the flagellum.

We use the Carreau constitutive model (Carreau, De Kee, & Chhabra, 1997) to investigate the undulatory motion in an inelastic shear-thinning fluid
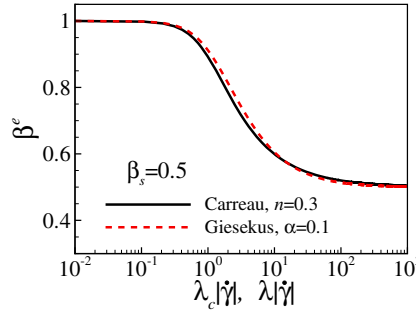
Figure 1. Shear-dependent viscosity of Carreau and Giesekus models in a simple shear flow.

$$\boldsymbol{\tau} = \beta^e \dot{\boldsymbol{\gamma}}, \tag{2a}$$

$$\beta^e = \beta_s + (1 - \beta_s)(1 + Cu^2|\dot{\gamma}|^2)^{\frac{n-1}{2}}, \quad (0 < n \le 1) \tag{2b}$$

where β_e is the normalized effective viscosity, β_s is the ratio of the solvent viscosity to the zero-shear-rate viscosity of the solution, $|\dot{\gamma}| = \sqrt{\dot{\boldsymbol{\gamma}} : \dot{\boldsymbol{\gamma}}/2}$ is the effective shear rate. The Carreau number $Cu = \lambda_c/T$ is the ratio between the characteristic time scale λ_c of the solution and the typical flow time scale T, where λ_c is the inverse of the shear rate at which the fluid transitions from Newtonian-like to power-law behaviour. The power-law index n determines how fast the viscosity decreases with shear rate. The larger n is, the slower the viscosity thins. At $\beta_s = 1$, $Cu = 0$, or $n = 1$, the model recovers to the Newtonian fluid. In all our simulations, we set $\beta_s = .5$ and $n = .3$.

To model the elasticity and shear-thinning properties of biological fluids, we use the Giesekus constitutive relation (Giesekus, 1982), in which $\boldsymbol{\tau}$ can be split into solvent and polymer contributions as $\boldsymbol{\tau} = \boldsymbol{\tau}^s + \boldsymbol{\tau}^p$, where $\boldsymbol{\tau}^s = \beta_s \dot{\boldsymbol{\gamma}}$,

$$\boldsymbol{\tau}^p + De \stackrel{\triangledown}{\boldsymbol{\tau}^p} + \frac{De\,\alpha}{1 - \beta_s}\boldsymbol{\tau}^p \cdot \boldsymbol{\tau}^p = (1 - \beta_s)(\nabla\mathbf{u} + \nabla\mathbf{u}^{\mathrm{T}}), \tag{3}$$

The Deborah number $De = \lambda/T$ is the ratio of the polymer relaxation time λ to the characteristic flow time scale T. Same viscosity ratio $\beta_s = .5$ is used for the Giesekus fluid. The mobility factor α, which is in the range of 0–1/2, represents the anisotropic hydrodynamic drag exerted on the polymer molecules by the surrounding solute molecules and affects the viscosity of the polymeric solution. At $\alpha = 0$, the Giesekus constitutive equation recovers to the Oldroyd-B model and has a constant viscosity. The notation $\stackrel{\triangledown}{\mathbf{A}}$ represents the upper-convected derivative,

$$\stackrel{\triangledown}{\mathbf{A}} = \frac{\partial\mathbf{A}}{\partial t} + \mathbf{u} \cdot \nabla\mathbf{A} - \nabla\mathbf{u}^{\mathrm{T}} \cdot \mathbf{A} - \mathbf{A} \cdot \nabla\mathbf{u}. \tag{4}$$

In a simple shear flow of Giesekus fluid, the effective viscosity is (Bird, Armstrong, & Hassager, 1987)

$$\beta^e = \beta_s + (1 - \beta_s)\frac{(1 - k)^2}{1 + (1 - 2\alpha)k}, \tag{5}$$

where $k = [1 - \chi]/[1 + (1 - 2\alpha)\chi]$ and $\chi^2 = [(1 + 16\alpha(1 - \alpha)De^2|\dot{\gamma}|^2)^{1/2} - 1]/$ $[8\alpha(1 - \alpha)De^2|\dot{\gamma}|^2]$. We set $\alpha = .1$ for the Giesekus model. In this case, the effective viscosity of Giesekus fluid behaves similarly as the Carreau model of $n = .3$, as shown in Figure 1. In biological materials, such as biofilm and mucus, λ and λ_c vary from O(1) to O(10^3) s, n from .1 to .9, and β_s from O(10^{-3}) to O(10^{-1}). The typical beating frequency of the flagellum ranges from 2 to 50 Hz. Therefore, for micro-organisms, De and Cu vary in a very wide range, from O(1) to O(10^4).

2.2. Numerical method

Simulations are conducted using a finite volume method on a fixed staggered grid implemented in the code developed by Dabiri and coworkers (Dabiri & Bhuvankar, 2016; Dabiri, Doostmohammadi, Bayareh, & Ardekani, 2015; Dabiri, Lu, & Tryggvason, 2013; Dabiri & Tryggvason, 2015). A conventional operator-splitting method is applied to enforce the continuity equation. The spatial derivatives in the convection term are evaluated using the Quadratic Upstream Interpolation for Convective Kinetics scheme and the diffusion terms are discretized using the central difference scheme. The viscoelastic stress is solved using a commonly used formulation denoted as elastic and viscous stresses splitting method (Guénette & Fortin, 1995). The computational domain is 1.24 × 20 with the grid size being $\Delta x = .01$ uniform in x-direction and in the region $y < 3$, where the flagellum motion occurs, and is gradually stretched outside this region. The time step is $\Delta t = 10^{-3}$ and a second-order total variation diminishing Runge–Kutta method is used for time marching. At the bottom boundary at $y = 0$, a no-slip boundary condition is imposed. Periodic boundary conditions are imposed at the left and right sides of the computational domain and far-field boundary conditions are imposed at the top boundary. The flagellum is modelled using a series of Lagrangian points immersed inside the fluid domain. The forcing term along the flagellum is calculated iteratively to impose the prescribed undulatory velocity and is then distributed back to the fluid (Ardekani et al., 2008). The details of the numerical method and validations can be found in our previous publications (Ardekani et al., 2008; Li & Ardekani, 2014).

When the swimmer approaches the wall, the high pressure in the thin film between the swimmer and the wall prevents any unphysical overlaps. However, a very small grid resolution is needed to properly capture this dynamic process and consequently it is computationally expensive. A short-range repulsive force (Glowinski, Pan, Hesla, Joseph, & Periaux, 2001) is added if the distance of any point on the swimmer from the wall is smaller than a certain value
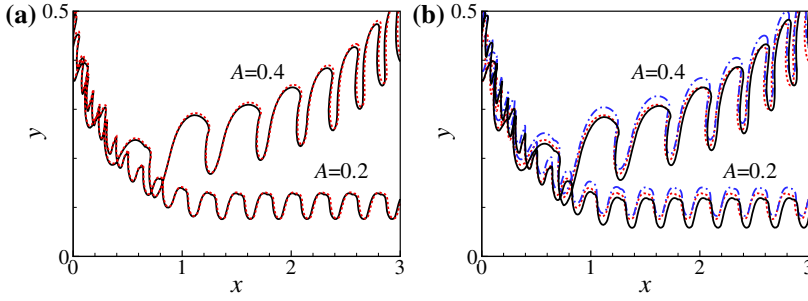
Figure 2. Trajectory of a near-wall kicker in a Newtonian fluid for (a) two different domain lengths, solid lines: $L_x = 10.24$ and dashed lines: $L_x = 20.48$ and (b) different repulsive forces, solid lines: $\varepsilon = 10^{-3}$, dashed lines: $\varepsilon = 10^{-4}$ and dashdot lines: $\varepsilon = 10^{-5}$.

$$F_r = \frac{F_R}{\varepsilon}\left(\frac{d - dr}{dr}\right)^2 e_z, \tag{6}$$

where F_R is the characteristic force, $\varepsilon = 10^{-4}$ is a small positive number, d is the distance between the point on the swimmer and the wall, dr is the force range and is usually set to the smallest grid size Δx in the computational domain (Glowinski et al., 2001). The direction of the repulsive force e_z is normal to the wall. In Figure 2, we investigate the effects of the length of periodic domain and the repulsive force on the results. The near-wall motion of flagellum is not sensitive to the choice of these parameters.

3. Near-wall motion in a Newtonian fluid

We first investigate the near wall swimming motion of a flagellum in a Newtonian fluid. Initially, the flagellum is located above the wall at $y_0 = .5$, with an initial angle $\theta_0 = -45°$. Here, θ is measured with respect to the direction parallel to the wall, and the swimmer is heading towards the wall for $\theta < 0$. Figure 3 compares the trajectory of the centre of the swimmer ($s = l/2$) undulating with different amplitudes. The high frequency oscillations correspond to the motion of the swimmer's centre in each undulatory cycle. Three different near-wall swimming modes are observed for the kicker. At $A \leq .3$, the kicker is stably attracted to the wall. The kicker swims close to the wall and periodically collides with it. This type of near-wall motion of an undulatory swimmer has been observed in simulations (Evans & Lauga, 2010) and experiments for a sperm (Kantsler, Dunkel, Polin, & Goldstein, 2013). At $A = .35$, the kicker is weakly attracted to the wall and swims in a cyclic trajectory. The kicker stays near the wall in a few undulatory cycles and quickly escapes, and it takes a much longer time for the swimmer to swim back towards the wall. The average distance between the kicker and the wall is on the order of the swimmer size which is consistent with the results of Smith et al. (2009). Similar cyclic near-wall motion was also observed for a puller squirmer near a wall (Li & Ardekani, 2014). At high enough
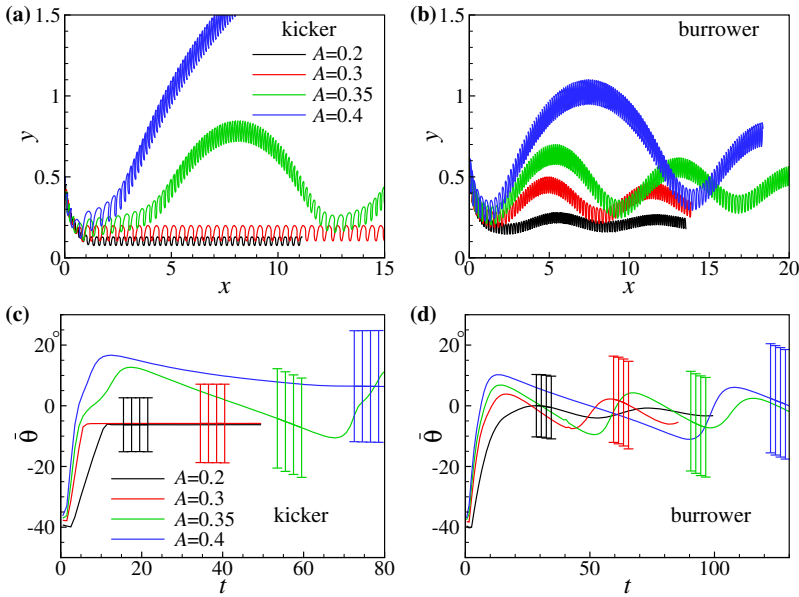
Figure 3. Trajectory of a near-wall (a) kicker and (b) burrower of different amplitudes in a Newtonian fluid. The swimmer is initially located at $y_0 = .5$ and $\theta_0 = -45°$. Time history of the orientation angle $\bar{\theta}$ averaged over an undulatory cycle for a (c) kicker and (d) burrower.
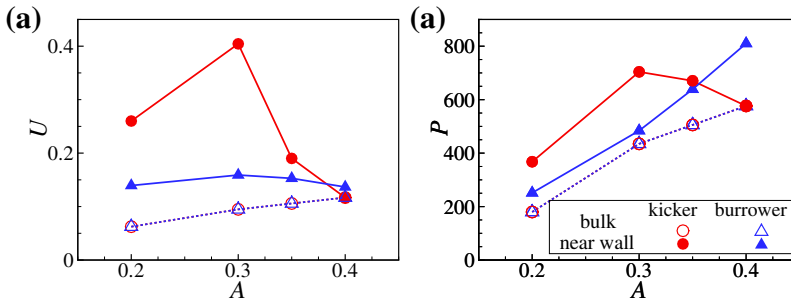Note: Error bars show the range of temporal variation of the angles.

Figure 4. (a) The swimming speed U and (b) power consumption P of swimmers in a Newtonian fluid as a function of the swimmer's amplitude A.

amplitude, the kicker eventually escapes the wall. Therefore, the wall attraction of an undulatory flagellum is strongly affected by its undulation amplitude. The burrower is weakly attracted to the wall and swims in a cyclic motion. The amplitude of its cyclic trajectory slowly decreases with time. Wall attraction is weakened at higher amplitudes for both swimmer types.

The weak attraction of an undulatory swimmer towards the wall can be understood in the light of the orientational angle of the swimmer. Figures 3(c) and (d) show the time history of the swimmer's angle averaged over an undulatory cycle, and error bars show the range of its temporal variation. As the swimmer approaches the wall, its head first contacts with the wall and the angle of the

swimmer quickly increases. For the kickers of $A = .2$ and $.3$, the final average angle is negative $\bar{\theta} \simeq -6°$ and the kicker is stably attracted to the wall. In this swimming mode, both the head and the tail of the kicker periodically collide with the wall. For a kicker with larger amplitudes, its scattering angle becomes positive, meaning the swimmer first escapes the wall after the collision and then swims back to the surface. Positive scattering angle is also observed for the burrower, and the wall effect slowly reduces the angle of the swimmer. Note that for a swimmer with large amplitudes, for example kicker of $A = .35$, there is no contact between the swimmer's tail and the wall, and the hydrodynamic interaction is responsible for the swimmer's attraction towards the wall after the first escape. The strength of this hydrodynamic interaction determines the near-wall swimming mode of the swimmer. For a kicker of $A = .35$ and a burrower with different undulation amplitudes, the orientation angle becomes negative and the swimmer comes back to the wall. For a kicker of $A = .4$, its initial scattering angle is large and the wall hydrodynamic effect becomes negligible before it can reorient the swimmer towards the wall. Therefore, the wall contact, the initial scattering angle of the swimmer and the hydrodynamic effects are all important to the near-wall motion of an undulatory swimmer.

The wall attraction strongly affects the swimming performance of an undulatory flagellum. In Figure 4, the swimming speed and the power consumption of swimmer in a bulk fluid and near a wall are compared. The power consumption is calculated by $P = \int_S \boldsymbol{u} \cdot \boldsymbol{f} \, dS$. In the bulk fluid, the swimming speed and the power consumption monotonically increase with the swimmer's amplitude. Due to symmetry, the performance of kickers and burrowers is exactly the same. The wall attraction increases the swimming speed as well as the power consumption compared to a swimmer in the bulk fluid. The effects are stronger for a swimmer closer to the wall. These results are consistent with an infinitely long flagellum near a wall (Katz, 1974). For both swimmer types, the maximum swimming speed occurs at $A = .3$. For the kicker, the near-wall swimming speed is about four times its speed in a bulk fluid, and its power consumption increases about 60%. These results indicate that the undulatory swimmer can optimise its swimming performance near the wall by tuning its undulation amplitude.

4. Near-wall motion in non-Newtonian fluids

Figure 5(a) and (b) compare the trajectories of a swimmer of $A = .2$ and $.4$ in Newtonian and inelastic shear-thinning fluids. The swimmer is initially located at $y_0 = .5$ and $\theta_0 = -45°$. Stronger wall attraction is observed for both kicker and burrower in an inelastic shear-thinning fluid. The kicker of $A = .4$ no longer escapes the wall and it swims in a cyclic trajectory in a shear-thinning fluid at $Cu = 1$. Further increase in the Carreau number to $Cu = 3$ does not affect kicker's trajectory. The shear-thinning effect decreases the distance of a burrower from the wall and a stable attraction is observed for burrower of
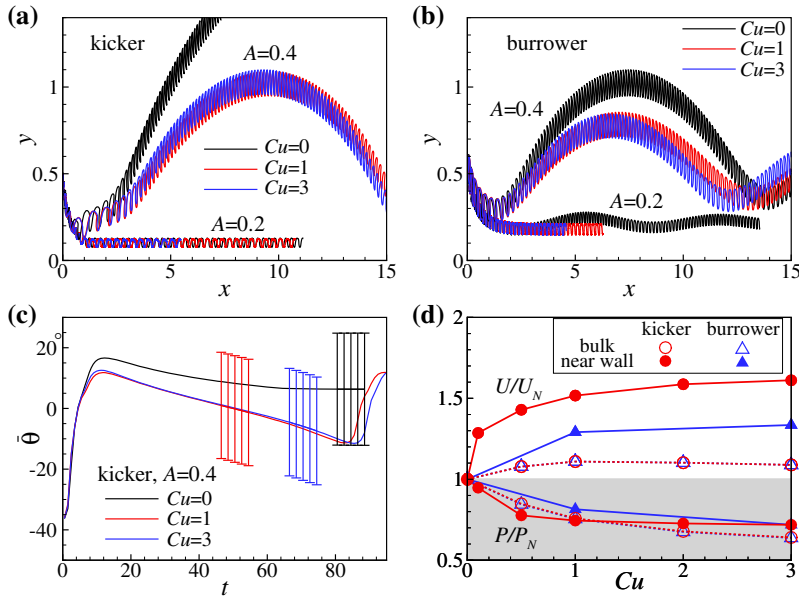
Figure 5. Trajectory of a near-wall swimming (a) kicker and (b) burrower of $A = .2$ and $.4$ in an inelastic shear-thinning fluid at $Cu = 1$. (c) Time history of the orientation angle $\bar{\theta}$ averaged over each undulatory cycle for a swimmer of $A = .4$. (d) The normalized swimming speed U/U_N and power consumption P/P_N of swimmers of $A = .2$ swimming in a bulk fluid and near a wall. Note: Here, U_N and P_N are the swimming speed and power consumption in a Newtonian fluid, respectively.

$A = .2$. The strong wall attraction is mainly related to the scattering angle of the swimmer. The shear-thinning viscosity decreases the scattering angle of the swimmer from the wall (see Figure 5(c)). Therefore, it stays near the wall for a longer time. In Figure 5(d), we compare the normalized speed and power of a stably attracted swimmer of $A = .2$ for different values of Carreau numbers. For both swimmer types, the shear-thinning effects increase the swimming speed and reduce the power consumption, no matter whether the swimmer is in the bulk fluid or near the wall. The shear-thinning effects are the same for a kicker and burrower in the bulk fluid. The speed reaches a peak at $Cu \sim 1$ as the swimmer moves in a corridor of low-viscosity fluids generated by large shear rates near an undulatory flagellum as demonstrated in our previous work (Li & Ardekani, 2015). When attracted to the wall, the swimmer's speed monotonically increases with increasing Cu. This speed enhancement is stronger for a swimmer near a wall. The power consumption roughly follows the same trend as the swimmer in the bulk fluid (Li & Ardekani, 2015).

The fluid elasticity strongly affects the wall attraction of the swimmer. Stable wall attraction of a kicker of $A = .2$ is observed in a viscoelastic fluid at $De = 1$ and $\alpha = 0$ (see Figure 6(a)). Compared to the swimmer in a Newtonian fluid, the kicker in a viscoelastic fluid of $De = 1$ and $\alpha = 0$ has a larger distance from the wall. Later, we will see that this is due to the fact that the kicker has a large orientation angle towards the wall in a constant-viscosity viscoelastic
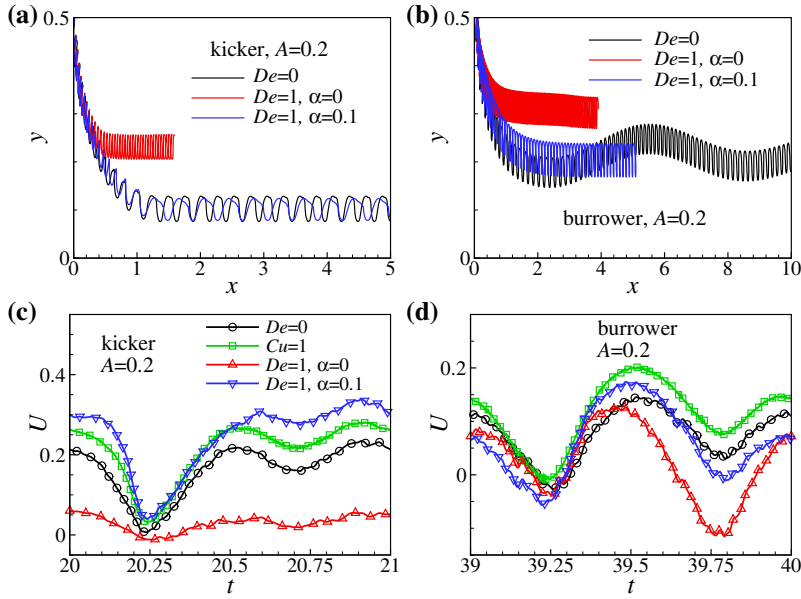
Figure 6. The trajectory of a near-wall swimming (a) kicker and (b) burrower of $A = .2$ in Newtonian and viscoelastic fluids. Comparison of the swimming speed of a near-wall swimming (c) kicker and (d) burrower in different fluids.

fluid. The fluid elasticity has same effects on the burrower, and a stable wall attraction is observed for a burrower in viscoelastic fluids (see Figure 6(b)). The non-Newtonian rheological behaviour of the background fluid has similar effects on the wall attraction of a kicker and a burrower, but their effects on the swimming speed are different. In Figure 6(c), we compare the temporal evolution of the swimming speed of a kicker of $A = .2$ in different fluids along the wall during an undulatory cycle. The instantaneous speed of the swimmer depends on its undulatory phase and the waveform near the wall. The non-Newtonian fluid behaviour does not qualitatively affect the temporal evolution of swimming speed, but it strongly affects the average swimming speed. The kicker swims much slower in a constant-viscosity viscoelastic fluid. Interestingly, the combination of the fluid elasticity and the shear-thinning viscosity strongly increases the swimming speed, which is larger than the one in an inelastic shear-thinning fluid. Such a speed enhancement in a shear-thinning viscoelastic fluid is not observed for a burrower.

The polymer molecules are highly stretched in the region near the head of the swimmer in a constant-viscosity viscoelastic fluid, which lead to a strong attraction of the swimmer towards the wall (see Figures 7(a) and (b)). On the other hand, this effect reduces the wall contact force on the swimmer's head and prevents the swimmer from further reorienting its angle away from the wall. This result is consistent with our previous finding on the wall attraction of a pusher squirmer in a viscoelastic fluid (Li et al., 2014). This large negative
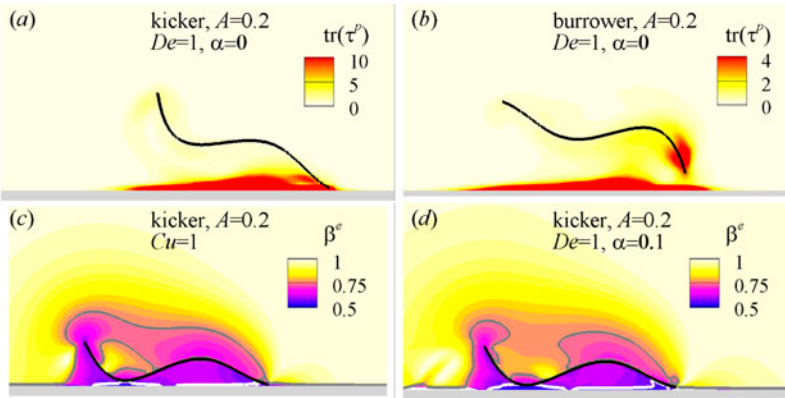
Figure 7. Polymer stretching around a near-wall swimming (a) kicker and (b) burrower of $A = .2$ in a viscoelastic fluid at $De = 1$ and $\alpha = 0$. The local fluid viscosity around a near-wall swimming kicker of $A = .2$ in (c) an inelastic shear-thinning fluid at $Cu = 1$ and (d) shear-thinning viscoelastic fluid at $De = 1$ and $\alpha = .1$ are shown.

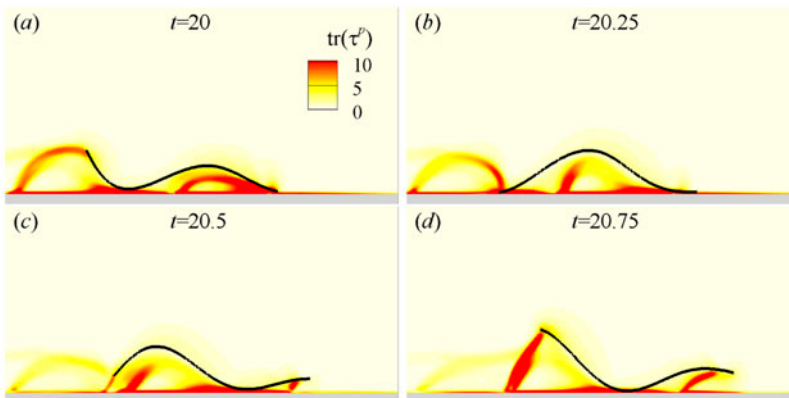Note: White and grey curves in (c) and (d) are the contour lines of $\beta^e = .55$ and .75, respectively.

Figure 8. Time sequence of the polymer stretching around a near-wall swimming kicker of $A = .2$ in a shear-thinning viscoelastic fluid at $De = 1$ and $\alpha = .1$.

angle lead to slower swimming speed. The undulatory motion of the kicker in an inelastic shear-thinning fluid locally reduces the effective viscosity of the fluid, creating a low viscosity fluid region around the flagellum and leading to an enhanced swimming speed (see Figure 7(c)). The fluid viscosity on the wall side is much more reduced due to the strong shear rate in the gap region. Therefore, the wall attraction due to fluid elasticity and the shear-thinning effects lead to a strong speed enhancement for an undulatory swimmer as shown in Figure 5(d). The distribution of effective viscosity in a shear-thinning viscoelastic fluid around the kicker, calculated using Equation (5), is similar to an inelastic shear-thinning fluid (see Figure 7(d)). On the wall side, the shear-thinning effect in a viscoelastic fluid is stronger than the inelastic shear-thinning fluid. On the other side, the size of the low-fluid viscosity region around the kicker is

smaller in a viscoelastic fluid. Both these effects lead to the speed enhancement of the swimmer as seen in Figure 6(c). Another reason for the stronger speed enhancement of a kicker in a shear-thinning viscoelastic fluid may be related to the effects of fluid elasticity. The polymer stretching around a kicker swimming near a wall is a highly dynamic process (see Figure 8). The undulatory motion of the head and the tail of the swimmer away from the wall strongly stretches the polymer molecules. As the swimmer swims along the wall, its entire body interacts with the polymer molecules stretched by its head. This interaction can lead to an attraction of the swimmer towards the wall which increases its swimming speed.

5. Summary and discussion

We have numerically investigated the near-wall motion of an undulatory swimmer of finite length in Newtonian and non-Newtonian fluids. In a Newtonian fluid, three types of near-wall swimming modes are observed for the kicker depending on the amplitude of the undulatory flagellum. The kicker of small amplitude is stably attracted to the wall and its speed is enhanced along the wall. In this type of swimming mode, both the head and the tail of the swimmer are in close contacts with the wall and the swimmer has a small negative angle towards the wall. This result is consistent with the observations of the near-wall swimming sperm (Elgeti et al., 2010). The swimming speed and the power consumption are greatly increased by the wall attraction. At larger amplitudes, the kicker first escapes from the wall. The hydrodynamic interaction between the swimmer and the wall reorients the swimmer back towards the wall. It may then swim in a cyclic trajectory. The swimmer is weakly attracted to the wall with its distance from the wall on the same order as the swimmer size. This attraction is observed in simulation results of Smith et al. (2009). The kicker escapes the wall for large enough initial scattering angle. Cyclic trajectories are observed for the burrowers studied in this work. These results show that both the flagella contact with the wall and the hydrodynamic interactions are crucial in determining the near-wall behaviour of an undulatory swimmer.

Non-Newtonian fluid rheology affects both the wall attraction and the swimming performance of the swimmer near the wall. Shear-thinning viscosity of the fluid slightly enhances the wall attraction, mainly by reducing the scattering angle of the swimmer. It greatly increases the swimming speed by creating a low-viscosity fluid region around the swimmer. This mechanism is the same as swimming in the bulk fluid. The effects of fluid elasticity are more complex. In a constant-viscosity viscoelastic fluid, it enhances the wall attraction by generating a strong polymer stretching region near the head of the swimmer and inhibits the swimmer's reorientation. As a result, the swimmer's head is strongly attracted to the wall and swims slowly with a high inclination angle along the wall. In a shear-thinning viscoelastic fluid, the combination of the fluid elasticity

and shear-thinning viscosity generates the strongest speed enhancement for the kicker. In this case, both the reduced viscosity near the swimmer and the interaction between the swimmer and the polymer molecules contribute to the speed enhancement. This strong speed enhancement is closely related to the undulation pattern of the near-wall swimmer and is not observed for the burrower. Cervical mucus has been shown to have both shear-thinning viscosity (Hwang et al., 1969) and elasticity (Wolf et al., 1977). Our results suggest that these properties lead to fast swimming motion of sperms near a wall in a shear-thinning viscoelastic fluid.

In the current study, the swimmer is modelled as a finite-length flagellum with a prescribed travelling wave form. The effects of non-Newtonian fluid rheology and wall contact on the undulation kinematics are not considered. Gagnon et al. have showed that the beating kinematics of a *C. elegans* in a shear-thinning fluid is the same as in a Newtonian fluid (Gagnon et al., 2014). The fluid elasticity, on the other hand, strongly influences the beating pattern of *Chlamydomonas* flagella (Qin, Gopinath, Yang, Gollub, & Arratia, 2015). The beating shape of *Chlamydomonas* flagella can also be modified by the wall contact, while the beating shape of a sperm is relatively less affected (Kantsler et al., 2013). The experimental results show that the swimming speed of the *C. elegans* in a Newtonian and shear-thinning fluid is the same (Gagnon et al., 2014). The present numerical results, on the other hand, predict a speed enhancement in the shear-thinning fluid. The difference may be due to the limit on the power consumption of the swimmer in experiments, which is not included in the present simulations. Further studies are required to include these effects, which could have important roles on the near-wall behaviour of a swimmer.

Disclosure statement

Funding

References

Ardekani, A., Dabiri, S., & Rangel, R. (2008). Collision of multi-particle and general shape objects in a viscous fluid. *Journal of Computational Physics, 227*, 10094–10107.

Ardekani, A., Joseph, D., Dunn-Rankin, D., & Rangel, R. (2009). Particle-wall collision in a viscoelastic fluid. *Journal of Fluid Mechanics, 633*, 475–483.

Ardekani, A., Rangel, R., & Joseph, D. (2007). Motion of a sphere normal to a wall in a second-order fluid. *Journal of Fluid Mechanics, 587*, 163–172.

Berke, A. P., Turner, L., Berg, H. C., & Lauga, E. (2008). Hydrodynamic attraction of swimming microorganisms by surfaces. *Physical Review Letters, 101*, 038102-1–038102-4.

Bird, R. B., Armstrong, R. C. & Hassager, O. (1987). *Dynamics of polymeric liquids. Vol. 1: Fluid mechanics*. New York, NY: John Wiley and Sons Inc.

Carreau, P. J., De Kee, D., & Chhabra, R. P. (1997). *Rheology of polymeric systems: Principles and applications*. Munich: Hanser Publishers.

Chrispell, J., Fauci, L., & Shelley, M. (2013). An actuated elastic sheet interacting with passive and active structures in a viscoelastic fluid. *Physics of Fluids, 25*, 013103-1–013103-16.

Curtis, M., Kirkman-Brown, J., Connolly, T., & Gaffney, E. (2012). Modelling a tethered mammalian sperm cell undergoing hyperactivation. *Journal of Theoretical Biology, 309*, 1–10.

Dabiri, S., & Bhuvankar, P. (2016). Scaling law for bubbles rising near vertical walls. *Physics of Fluids, 28*, 062101-1–062101-13.

Dabiri, S., Doostmohammadi, A., Bayareh, M., & Ardekani, A. (2015). Rising motion of a swarm of drops in a linearly stratified fluid. *International Journal of Multiphase Flow, 69*, 8–17.

Dabiri, S., Lu, J., & Tryggvason, G. (2013). Transition between regimes of a vertical channel bubbly upflow due to bubble deformability. *Physics of Fluids, 25*, 102110-1–102110-12.

Dabiri, S., & Tryggvason, G. (2015). Heat transfer in turbulent bubbly flow in vertical channels. *Chemical Engineering Science*, *122*, 106–113.

Datt, C., Zhu, L., Elfring, G. J., & Pak, O. S. (2015). Squirming through shear-thinning fluids. *Journal of Fluid Mechanics, 784*, R1-1–R1-11.

Drescher, K., Dunkel, J., Cisneros, L. H., Ganguly, S., & Goldstein, R. E. (2011). Fluid dynamics and noise in bacterial cell-cell and cell-surface scattering. *Proceedings of the National Academy of Sciences of the United States of America, 108*, 10940–10945.

Elgeti, J., Kaupp, U. B., & Gompper, G. (2010). Hydrodynamics of sperm cells near surfaces. *Biophysical Journal, 99*, 1018–1026.

Elgeti, J., Winkler, R. G., & Gompper, G. (2015). Physics of microswimmerssingle particle motion and collective behavior: A review. *Reports on Progress in Physics, 78*, 056601-1–056601-50.

Evans, A. A., & Lauga, E. (2010). Propulsion by passive filaments and active flagella near boundaries. *Physical Review E, 82*, 041915-1–041915-12.

Gagnon, D., & Arratia, P. (2016). The cost of swimming in generalized Newtonian fluids: Experiments with *C. elegans*. *Journal of Fluid Mechanics, 800*, 753–765.

Gagnon, D. A., Keim, N. C., & Arratia, P. E. (2014). Undulatory swimming in shear-thinning fluids: Experiments with *Caenorhabditis elegans*. *Journal of Fluid Mechanics, 758*, R3-1–R3-11.

Giesekus, H. (1982). A simple constitutive equation for polymer fluids based on the concept of deformation-dependent tensorial mobility. *Journal of Non-Newtonian Fluid Mechanics, 11*, 69–109.

Glowinski, R., Pan, T., Hesla, T., Joseph, D., & Periaux, J. (2001). A fictitious domain approach to the direct numerical simulation of incompressible viscous flow past moving rigid bodies: Application to particulate flow. *Journal of Computational Physics, 169*, 363–426.

Guénette, R., & Fortin, M. (1995). A new mixed finite element method for computing viscoelastic flows. *Journal of Non-Newtonian Fluid Mechanics, 60*, 27–52.

Guy, R. D., & Thomases, B. (2015). Computational challenges for simulating strongly elastic flows in biology. In S.E. Spagnolie (Ed.), *Complex fluids in biological systems* (pp. 359–397). New York, NY: Springer.

Hall-Stoodley, L., Costerton, J. W., & Stoodley, P. (2004). Bacterial biofilms: From the natural environment to infectious diseases. *Nature Reviews Microbiology, 2*, 95–108.

Harman, M. W., Dunham-Ems, S. M., Caimano, M. J., Belperron, A. A., Bockenstedt, L. K., Fu, H. C., et al. (2012). The heterogeneous motility of the lyme disease spirochete in gelatin

mimics dissemination through tissue. *Proceedings of the National Academy of Sciences of the United States of America, 109*, 3059–3064.

Hwang, S., Litt, M., & Forsman, W. (1969). Rheological properties of mucus. *Rheologica Acta, 8*, 438–448.

Ishimoto, K., & Gaffney, E. A. (2014). A study of spermatozoan swimming stability near a surface. *Journal of Theoretical Biology, 360*, 187–199.

Kantsler, V., Dunkel, J., Polin, M., & Goldstein, R. E. (2013). Ciliary contact interactions dominate surface scattering of swimming eukaryotes. *Proceedings of the National Academy of Sciences of the United States of America, 110*, 1187–1192.

Katz, D. F. (1974). On the propulsion of micro-organisms near solid boundaries. *Journal of Fluid Mechanics, 64*, 33–49.

Lauga, E. (2007). Propulsion in a viscoelastic fluid. *Physics of Fluids, 19*, 083104-1–083104-13.

Lauga, E., DiLuzio, W. R., Whitesides, G. M., & Stone, H. A. (2006). Swimming in circles: Motion of bacteria near solid boundaries. *Biophysical Journal, 90*, 400–412.

Lauga, E., & Powers, T. R. (2009). The hydrodynamics of swimming microorganisms. *Reports on Progress in Physics, 72*, 096601-1–096601-36.

Li, G., & Ardekani, A. M. (2014). Hydrodynamic interaction of microswimmers near a wall. *Physical Review E, 90*, 013010-1–013010-12.

Li, G., & Ardekani, A. M. (2015). Undulatory swimming in non-Newtonian fluids. *Journal of Fluid Mechanics, 784*, R4-1–R4-13.

Li, G., Karimi, A., & Ardekani, A. M. (2014). Effect of solid boundaries on swimming dynamics of microorganisms in a viscoelastic fluid. *Rheologica Acta, 53*, 911–926.

Li, G., McKinley, G. H., & Ardekani, A. M. (2015). Dynamics of particle migration in channel flow of viscoelastic fluids. *Journal of Fluid Mechanics, 785*, 486–505.

Li, G., & Tang, J. X. (2009). Accumulation of microswimmers near a surface mediated by collision and rotational brownian motion. *Physical Review Letters, 103*, 078101-1–078101-4.

Martinez, V. A., Schwarz-Linek, J., Reufer, M., Wilson, L. G., Morozov, A. N., & Poon, W. C. (2014). Flagellated bacterial motility in polymer solutions. *Proceedings of the National Academy of Sciences of the United States of America, 111*, 17771–17776.

Montecucco, C., & Rappuoli, R. (2001). Living dangerously: How helicobacter pylori survives in the human stomach. *Nature Reviews Molecular Cell Biology, 2*, 457–466.

Montenegro-Johnson, T. D., Smith, A. A., Smith, D. J., Loghin, D., & Blake, J. R. (2012). Modelling the fluid mechanics of cilia and flagella in reproduction and development. *European Physical Journal E, 35*, 1–17.

Montenegro-Johnson, T. D., Smith, D. J., & Loghin, D. (2013). Physics of rheologically enhanced propulsion: Different strokes in generalized Stokes. *Physics of Fluids, 25*, 081903-1–081903-26.

Qin, B., Gopinath, A., Yang, J., Gollub, J. P., & Arratia, P. E. (2015). Flagellar kinematics and swimming of algal cells in viscoelastic fluids. *Scientific Reports, 5*, 9190-1–9190-7. DOI: 10.1038/srep09190.

Shen, X., & Arratia, P. E. (2011). Undulatory swimming in viscoelastic fluids. *Physical Review Letters, 106*, 208101-1–208101-4.

Rothschild, L. (1963). Non-random distribution of bull spermatozoa in a drop of sperm suspension. *Nature, 198*, 1221–1222.

Simons, J., Olson, S., Cortez, R., & Fauci, L. (2014). The dynamics of sperm detachment from epithelium in a coupled fluid-biochemical model of hyperactivated motility. *Journal of Theoretical Biology, 354*, 81–94.

Smith, D., Gaffney, E., Blake, J., & Kirkman-Brown, J. (2009). Human sperm accumulation near surfaces: A simulation study. *Journal of Fluid Mechanics, 621*, 289–320.

Spagnolie, S. E., & Lauga, E. (2012). Hydrodynamics of self-propulsion near a boundary: Predictions and accuracy of far-field approximations. *Journal of Fluid Mechanics, 700*, 105–147.

Suarez, S., & Pacey, A. (2006). Sperm transport in the female reproductive tract. *Human Reproduction Update, 12*, 23–37.

Taylor, G. (1951). Analysis of the swimming of microscopic organisms. *Proceedings of the Royal Society A, 209*, 447–461.

Teran, J., Fauci, L., & Shelley, M. (2010). Viscoelastic fluid response can increase the speed and efficiency of a free swimmer. *Physical Review Letters, 104*, 038101-1–038101-4.

Thomases, B., & Guy, R. D. (2014). Mechanisms of elastic enhancement and hindrance for finite-length undulatory swimmers in viscoelastic fluids. *Physical Review Letters, 113*, 098102-1–098102-5.

Vélez-Cordero, J. R., & Lauga, E. (2013). Waving transport and propulsion in a generalized Newtonian fluid. *Journal of Non-Newtonian Fluid Mechanics, 199*, 37–50.

Wolf, D. P., Blasco, L., Khan, M. A., & Litt, M. (1977). Human cervical mucus. *I. rheologic characteristics. Fertility and Sterility, 28*, 41–46.

Woolley, D. (2003). Motility of spermatozoa at surfaces. *Reproduction, 126*, 259–270.

Yazdi, S., Ardekani, A. M., & Borhan, A. (2014). Locomotion of microorganisms near a no-slip boundary in a viscoelastic fluid. *Physical Review E, 90*, 043002-1–043002-11.

Yazdi, S., Ardekani, A. M., & Borhan, A. (2015). Swimming dynamics near a wall in a weakly elastic fluid. *Journal of Nonlinear Science, 25*, 1153–1167.

Yuan, J., Raizen, D. M., & Bau, H. H. (2015). Propensity of undulatory swimmers, such as worms, to go against the flow. *Proceedings of the National Academy of Sciences of the United States of America, 112*, 3606–3611.